TISSUE ENGINEERING: Part A
Volume 21, Numbers 7 and 8, 2015
© Mary Ann Liebert, Inc.
DOI: 10.1089/ten.tea.2014.0288

Capillary-Like Network Formation by Human Amniotic Fluid-Derived Stem Cells Within Fibrin/Poly(Ethylene Glycol) Hydrogels

Omar M. Benavides, PhD,[1] Joseph P. Quinn, BS,[2] Seokwon Pok, PhD,[1] Jennifer Petsche Connell, PhD,[1] Rodrigo Ruano, MD, PhD,[3] and Jeffrey G. Jacot, PhD[1,4]

A major limitation in tissue engineering strategies for congenital birth defects is the inability to provide a significant source of oxygen, nutrient, and waste transport in an avascular scaffold. Successful vascularization requires a reliable method to generate vascular cells and a scaffold capable of supporting vessel formation. The broad potential for differentiation, high proliferation rates, and autologous availability for neonatal surgeries make amniotic fluid-derived stem cells (AFSC) well suited for regenerative medicine strategies. AFSC-derived endothelial cells (AFSC-EC) express key proteins and functional phenotypes associated with endothelial cells. Fibrin-based hydrogels were shown to stimulate AFSC-derived network formation *in vitro* but were limited by rapid degradation. Incorporation of poly(ethylene glycol) (PEG) provided mechanical stability (65% ± 9% weight retention vs. 0% for fibrin-only at day 14) while retaining key benefits of fibrin-based scaffolds—quick formation (10 ± 3 s), biocompatibility (88% ± 5% viability), and vasculogenic stimulation. To determine the feasibility of AFSC-derived microvasculature, we compared AFSC-EC as a vascular cell source and AFSC as a perivascular cell source to established sources of these cell types—human umbilical vein endothelial cells (HUVEC) and mesenchymal stem cells (MSC), respectively. Cocultures were seeded at a 4:1 endothelial-to-perivascular cell ratio, and gels were incubated at 37°C for 2 weeks. Mechanical testing was performed using a stress-controlled rheometer ($G' = 95 \pm 10$ Pa), and cell-seeded hydrogels were assessed based on morphology. Network formation was analyzed based on key parameters such as vessel thickness, length, and area, as well as the degree of branching. There was no statistical difference between individual cultures of AFSC-EC and HUVEC in regard to these parameters, suggesting the vasculogenic potential of AFSC-EC; however, the development of robust vessels required the presence of both an endothelial and a perivascular cell source and was seen in AFSC cocultures (70% ± 20% vessel length, 90% ± 10% vessel area, and 105% ± 10% vessel thickness compared to HUVEC/MSC). At a fixed seeding density, the coculture of AFSC with AFSC-EC resulted in a synergistic effect on network parameters similar to MSC (150% vessel length, 147% vessel area, 150% vessel thickness, and 155% branching). These results suggest that AFSC-EC and AFSC have significant vasculogenic and perivasculogenic potential, respectively, and are suited for *in vivo* evaluation.

Introduction

The clinical applications of tissue engineering are currently limited by the inability to provide a significant source of oxygen, nutrient, and waste transport to implanted constructs in the initial phase after implantation.[1] Both natural and engineered tissues more than 200 μm thick require suitable vascular support to maintain cell viability and function.[2] As a result, clinical success has generally been restricted to thin or avascular tissues, such as the bladder, cartilage, and skin.[3]

To address this requirement, previous studies have investigated factors and scaffolds that stimulate angiogenesis, driving invasion of host-derived blood vessels into implanted constructs[4] and prevascularized scaffolds, and generating microvascular networks *in vitro* before implantation.[5] Post-implantation, vascular ingrowth can occur in response to encapsulated cells experiencing hypoxia and secreting angiogenic cytokines or the addition of exogenous cytokines.

However, the development of new blood vessels is time intensive and can only be accelerated to a limited extent. The rate of spontaneous angiogenesis is on the order of

Departments of [1]Bioengineering and [2]Chemical and Biomolecular Engineering, Rice University, Houston, Texas.
[3]Maternal-Fetal Medicine, Baylor College of Medicine, Houston, Texas.
[4]Congenital Heart Surgery Services, Texas Children's Hospital, Houston, Texas.

tenths of a micron per day,[6] while chemotaxis-driven ingrowth has been estimated at several microns per hour.[7,8] The time to complete perfusion increases significantly with volume, during which hypoxia in the core of the implant, along with nutrient and oxygen gradients in the outer regions, could result in nonuniform cell viability and thus decreased tissue function.[9] On the other hand, prevascularization strategies generate microvascular networks within tissue before implantation, resulting in reperfusion driven by anastomosis rather than angiogenesis, and are much less dependent on scaffold size.[5]

The engineering of robust vascular structures requires both an endothelial cell source and a perivascular cell source, such as mesenchymal stem cells (MSC), dermal fibroblasts, or marrow stromal cells, which increase cell survival and proliferation.[10] Broad potential for differentiation, high proliferation rates, and ease of isolation make human amniotic fluid-derived stem cells (AFSC) well suited for regenerative medicine strategies.[11] AFSC could also prove to be a significant source for autologous therapies in neonates such as in an engineered cardiovascular patch for Tetralogy of Fallot repair[12] or to aid in vascular reconstruction of other congenital defects.[13] AFSC isolated and differentiated into endothelial cells in previous studies from our group express key endothelial molecular markers (vWF, eNOS, and CD31), display functional phenotypes associated with endothelial cells (nitric oxide production and ac-LDL uptake), and form networks when encapsulated in Matrigel,[14] all of which suggest vasculogenic potential. In addition, AFSC have a similar morphology, surface marker expression, and differentiation capacity compared to MSC, a proven source of perivascular cells, suggesting the potential use of AFSC as a vascular support cell source.[11,14–17]

Fibrin-based hydrogels stimulate vascularization and are used in clinical applications, such as growth factor delivery and cell encapsulation, making them an appropriate platform for assessing the vasculogenic potential of AFSC.[18] The main limitation associated with fibrin in tissue engineering is rapid degradation, which leads to loss of implant volume within days.[19] Incorporation of poly(ethylene glycol) (PEG), which is known for biocompatibility and tunable physical properties, allows for increased mechanical stability while retaining the key benefits of fibrin-based scaffolds—quick formation, biocompatibility, and angiogenic stimulation.[20] Based on these data, we hypothesized that a population of stem cells derived from human amniotic fluid (AF) and differentiated into endothelial cells could form cohesive vascular networks within a fibrin/PEG matrix. In this study, we compared the three-dimensional network formation by AFSC-derived endothelial cells (AFSC-EC) to that of a mature endothelial cell source, human umbilical vein endothelial cells (HUVEC), using quantitative assessment of morphometric and spatial vessel parameters.

Materials and Methods

Isolation of human AFSC

Primary human AF was obtained from patients in their second trimester undergoing planned amnioreduction as part of a therapeutic treatment for the twin-to-twin transfusion syndrome (TTTS) as previously described.[14] Collection from TTTS cases provides at least an eightfold increase in AF per patient compared to routine amniocentesis while maintaining a cell population with a normal karyotype. The experimental protocol and informed consent forms were approved by the Institutional Review Boards of Baylor College of Medicine and Rice University. Briefly, AF was centrifuged for 10 min at 150 rcf, and collected cells were plated at 2500 cells/cm^2 on standard plastic Petri dishes and cultured in modified α-Minimum Essential Media: 63% αMEM (Invitrogen, Carlsbad, CA), 18% Chang Basal Medium (Irvine Scientific, Santa Ana, CA), 2% Chang C supplement (Irvine Scientific), 15% fetal bovine serum (PAA Laboratories, Dartmouth, MA), and GlutaMAX (Invitrogen) at 37°C and 5% CO_2 in a humidified environment. Cells were passaged at 60–70% confluency and AFSC were isolated through fluorescence-activated cell sorting for expression of the membrane receptor CD117/c-kit (1:100 antibody concentration, BD Biosciences, Bedford, MA; Dako-Cytomation MoFlo sterile cell sorter).

Analysis of undifferentiated c-kit$^+$ AF cells

Standard G-banding karyotyping was performed on undifferentiated AFSC at passage 5. In addition, flow cytometry (BD LSR II Flow Cytometer) was performed to evaluate the expression of the embryonic stem cell markers SSEA4, Oct-4, Sox2, Tra-1-60/81, and c-myc and the MSC markers c-kit, CD29, CD44, CD73, CD90, and CD105. All flow cytometry antibodies and corresponding isotype controls were purchased from BD Biosciences, specific to human proteins, and used at manufacturer-recommended concentrations. Staining for intracellular markers was performed after fixing and permeabilizing cells. FACSDiva software (BD Biosciences) was used for all flow cytometry data collection. FlowJo software (Tree Star, Inc., Ashland, OR) was used for data analysis.

Endothelial differentiation of AFSC

AFSC were differentiated into endothelial-like cells as previously described. Briefly, c-kit$^+$ AFSC at passage 4 were plated at 3000 cells/cm^2 on gelatin-coated plates, allowed to attach for 24 h in modified αMEM, and then cultured in Endothelial Growth Media 2 (EGM-2; Lonza, Walkersville, MD) with a final concentration of 50 ng/mL vascular endothelial growth factor ($VEGF_{165}$; Pierce Biotechnology, Rockford, IL). EGM-2 contained epidermal growth factor, hydrocortisone, GA-1000 (gentamicin, amphotericin-b), fetal bovine serum, basic fibroblast growth factor, insulin-like growth factor, ascorbic acid, and heparin at manufacturer concentrations. Media were changed every 2 days, and the degree of differentiation was assessed after 14 days. HUVEC (courtesy of Joel Moake, Rice University) cultured in complete EGM-2 without supplemental VEGF were used as a positive control, while c-kit$^+$ AFSC in modified αMEM were used as a negative control. Both controls were analyzed at passage 5.

Postdifferentiation flow cytometry

Using the flow cytometry protocol and equipment described previously, differentiated AFSC were detached into single cells and stained with fluorescently conjugated antibodies. Targets and their respective isotype controls were as follows: CD31 (FITC IgG1κ), VE-cadherin (PE IgG1κ), VEGFR2 (AF647 IgG1), SSEA4 (PE IgG3κ), c-kit (PE

IgG1κ), HLA-DR (FITC IgG2b), and HLA-ABC (PE IgG1). All flow cytometry antibodies and corresponding isotype controls were purchased from BD Biosciences, specific to human proteins, and used at manufacturer-recommended concentrations. In addition, a subset of the differentiated population was sorted based on CD31 expression. This endothelial-like population was referred as AFSC-EC.

Production of fibrin/PEG hydrogels

Fibrin/PEG-based hydrogels were prepared based on work previously described.[20–22] Human fibrinogen (F3879; Sigma-Aldrich, St Louis, MO) was solubilized in phosphate-buffered saline (PBS, 21-030-CV; Corning, Manassas, VA; adjusted to pH 7.8) at a concentration of 80 mg/mL. After 2 h of incubation at 37°C and brief vortexing, the solution was sterilized using a 0.20-μm SteriFlip filter (EMD Millipore, Billerica, MA). Succinimidyl glutarate-modified bifunctional PEG (3.4 kDa SG-PEG-SG; NOF America Corporation, White Plains, NY) was dissolved in PBS at 8 mg/mL and syringe filtered. Fibrinogen and PEG solutions were combined in a 1:1 volume ratio, mixed thoroughly, and incubated at 37°C for 10 min. For low-concentration hydrogels, the solution was diluted 2:1 in PBS before incubation, maintaining the 10:1 fibrinogen:PEG ratio. PEGylated fibrinogen was then added into low-attachment PTFE molds and mixed at a 1:1 volume ratio with either PBS (for controls) or cell solution (200,000 cells/mL; cocultures seeded at a 4:1 endothelial-to-perivascular cell ratio). Human thrombin (T7009; Sigma-Aldrich) was diluted to 25 U/mL in sterile 40 mM CaCl2 (208291; CalBiochem, La Jolla, CA) and added 1:1 with the PEGylated fibrinogen/cell solution. Gelation occurred on the order of seconds, and gels were incubated at 37°C for 5–10 min before adding EGM-2. Media were changed after 30 min, 2 h, and then daily.

Characterization of fibrin/PEG hydrogels

Gelation time. Gelation of fibrin/PEG hydrogels at 37°C was measured by inverting gel solutions of the same stock sequentially at a rate of 1 Hz. Start time was defined as the addition of thrombin, and gelation time was defined as the point at which negligible liquid solution remained at inversion.

Stiffness. Mechanical testing of fibrin/PEG hydrogels was performed using a stress-controlled rheometer (Rheolyst AR1000; TA Instruments, New Castle, DE) in a cone–plate configuration (1° cone, 0.1 mm gap size, 0.5 Hz oscillatory shear strain frequency, 1% max strain amplitude). PEGylated fibrinogen solutions were added to the rheometer base, thrombin was added 1:1 as described in the Production of Fibrin/PEG Hydrogels section, and the postgelation storage modulus (G′) of the samples was obtained using the TA Instruments Rheology Advantage Software.

Morphology. The microstructure of fibrin/PEG hydrogels was analyzed using scanning electron microscopy (Nova NanoSEM 230; FEI, Hillsboro, OR). Hydrogels were fixed in 4% paraformaldehyde (Alfa Aesar, Ward Hill, MA), dehydrated using serial dilution in ethanol (EX0276-3; Millipore) up to 100%, and dried using a critical point dryer (K850; EMI Tech, Inc., Fall River, MA). Samples were then sputter coated (208HR; Cressington Scientific, Watford, England, United Kingdom) with a 5 nm thick layer of platinum. Scanning electron microscope (SEM) images were taken between 5.0–7.0 keV and 5–15k magnification using the xT Microscope Control software (FEI).

Degradation rate. Fibrin/PEG hydrogels were desiccated, and the degradation rate was measured as the dry weight retention normalized to initial weight ($Weight_{final}$/$Weight_{initial}$) versus time.

Cell viability. Viability of encapsulated cells was determined after 7 days using a LIVE/DEAD Cell Viability Assay (L34951; Life Technologies, Grand Island, NY) in which metabolically active cells are stained with a green-fluorescent small molecule and cells with compromised plasma membranes are stained with a red-fluorescent small molecule. Images were obtained using a DMI 6000B (Leica Microsystems, Bannockburn, IL) fluorescence microscope and Leica Application Suite software.

Assessment of network formation

Immunostaining. To observe the organization of encapsulated cells within the fibrin/PEG hydrogels, constructs were fixed with 4% paraformaldehyde, permeabilized with Triton X100 (CalBioChem), and stained with fluorescently conjugated phalloidin (A12379; Life Technologies). Using phalloidin to label f-actin throughout the cells provided a clear outline of the three-dimension structures formed and allows for semiautomated analysis of images. Images were taken using an LSM 510 META confocal microscope and accompanying LSM 5 Series software (Zeiss, Jena, Germany).

Network analysis. Images were analyzed using AngioTool, a free ImageJ package developed by the NIH National Cancer Institute. AngioTool outlines continuous networks within images, provides a skeletal representation of them, and allows for quantitative assessment of various vessel morphometric and spatial parameters, including vessel length, density, thickness, and branching index.

Assessment of lumen formation

Fibrin/PEG hydrogels were sectioned at the Baylor College of Medicine Breast Cancer Pathology core facility. Briefly, cells were fixed in 4% paraformaldehyde, serially dehydrated in ethanol, cleared with xylenes, and embedded in paraffin using the Sakura Tissue-Tek VIP Processor and Paraffin Embedding Center (Sakura FineTek USA, Inc., Torrance, CA). The scaffolds were then sectioned using an HM 315 microtome (Richard-Allan Scientific/Thermo Scientific, Waltham, MA) at a thickness of 3–4 μm. Hematoxylin and eosin (H&E) staining was done using a Shandon Varistain 24-4 Automatic Slide Stainer (Thermo Scientific). Immunofluorescent staining of αSMA (ab7817; Abcam, Cambridge, MA) and CD31 (ab28364; Abcam) was performed using heat-mediated, citrate-buffered antigen retrieval (ab973; Abcam). Imaging was done using an Eclipse E800 microscope and accompanying NIS-Elements software (Nikon Instruments, Inc., Melville, NY).

Statistical analysis

Data are expressed as mean ± standard deviation. The sample numbers for each experiment are represented in

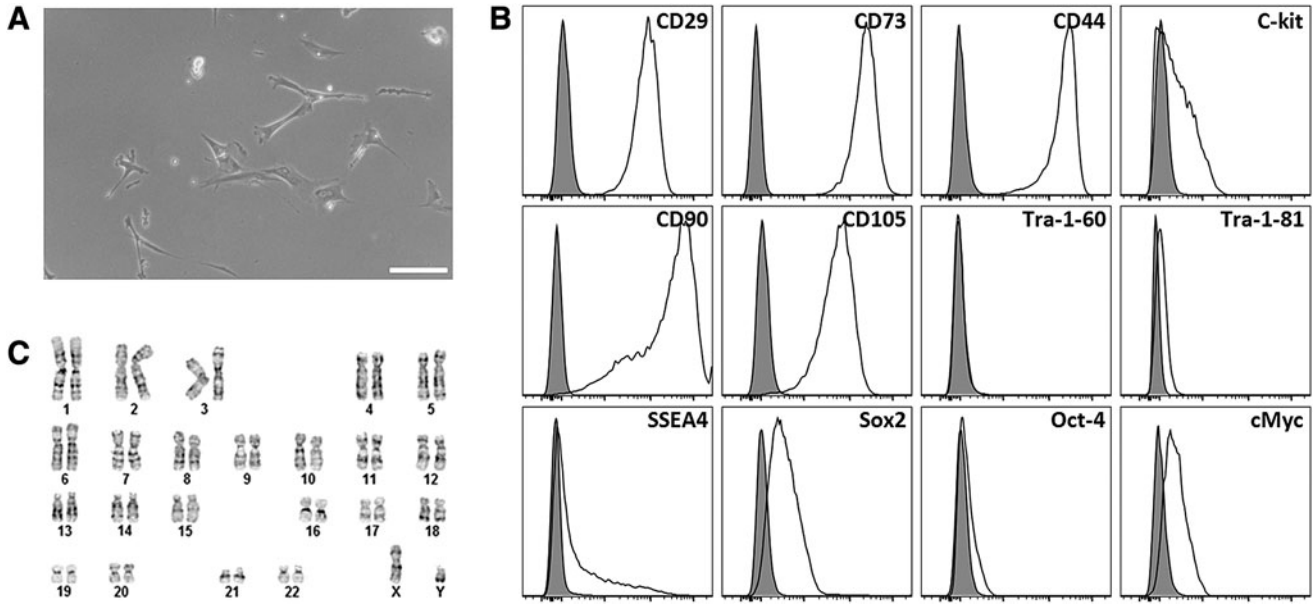

FIG. 1. Characterization of undifferentiated AFSC. AFSC were sorted for c-kit$^+$ at passage 2, cultured to passage 5, and analyzed. **(A)** Light microscopy revealed a spindle-shaped morphology similar to MSC. Scale bar is 100 μm. **(B)** Flow cytometry analysis showed that AFSC were strongly positive for the MSC markers CD29, CD44, CD73, CD90, and CD105; moderately positive for the ESC markers SSEA4, Sox2, and cMyc; and negative for the ESC marker Tra-1-60/81. Additionally, a subpopulation of these cells retained c-kit expression throughout passaging. **(C)** Standard G-banding karyotyping of AFSC shows a normal diploid male karyotype. AFSC, amniotic fluid-derived stem cells; MSC, mesenchymal stem cells.

their respective figures. Analysis of variance followed by a *post hoc* Student's *t*-test with a Dunn–Bonferroni correction for multiple comparisons was performed for all comparisons. A value of $p < 0.05$ was considered significant in all tests.

Results

Isolation and characterization of AFSC

Adherent AFSC were isolated from AF samples and had a fibroblast-like spindle-shaped morphology similar to that of

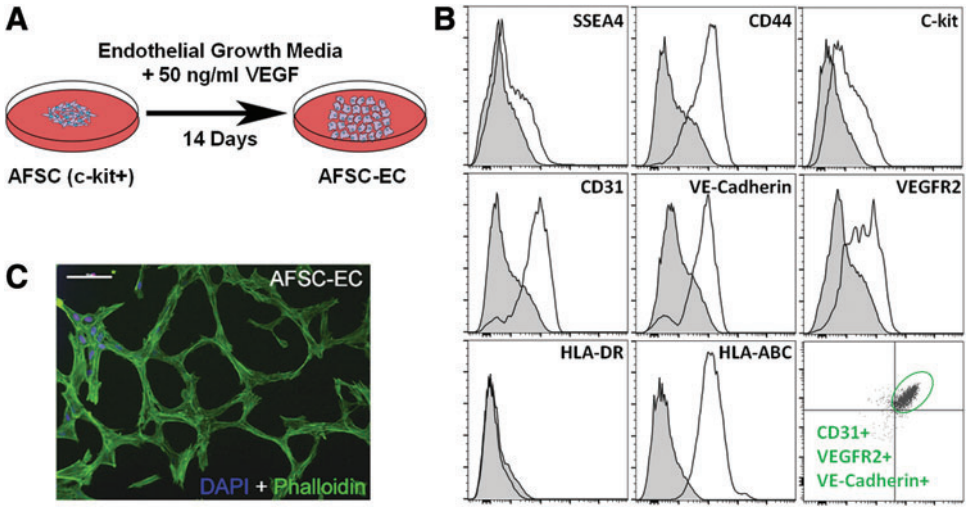

FIG. 2. Assessment of AFSC-derived endothelial cells (AFSC-EC). **(A)** Schematic of the vascular endothelial growth factor (VEGF)-mediated differentiation of c-kit$^+$ AFSC into AFSC-EC. **(B)** Flow cytometry analysis of AFSC-EC showed significant expression of constitutive endothelial proteins such as CD31, VE-cadherin, and VEGFR2, although did not show a complete reduction in the stem cell markers SSEA4, c-kit, or CD44. Differentiated cells were negative for the immunological marker HLA-DR and positive for HLA-ABC. Additionally, a population of CD31$^+$ cells (16.4%) was also positive for both VE-cadherin and VEGFR2 (*bottom right panel*). **(C)** Fluorescence imaging of two-dimensional network formation of AFSC-EC when plated on a thin Matrigel film. Actin filaments were labeled with phalloidin (*green*) and nuclei were counterstained with DAPI (*blue*). Scale bar is 100 μm. Color images available online at www.liebertpub.com/tea

MSC (Fig. 1A). Flow cytometry on undifferentiated AFSC sorted for c-kit at passage 2 and then cultured through passage 5 showed that the cells were strongly positive for the MSC markers CD29 (99.7%), CD44 (99.4%), CD73 (99.9%), CD90 (95.3%), and CD105 (95.8%); moderately positive for the ESC markers SSEA4 (25.6%), Sox2 (32.6%), and cMyc (22.5%); and negative for the ESC marker Tra-1-60/80 (0.18%, 0.60%). In addition, a subpopulation (19.8%) of these cells retained c-kit expression through passaging (Fig. 1B). Standard G-banding karyotyping revealed a normal diploid male karyotype in all metaphase spreads (Fig. 1C).

Assessment of endothelial differentiation

Differentiation of AFSC into endothelial-like cells (AFSC-EC) was chemically mediated by the addition of 50 ng/mL VEGF to AFSC cultures (Fig. 2A). Flow cytometry was used to quantify protein expression (Fig. 2B), while the ability to form networks in two dimensions was confirmed by plating the AFSC-EC on a thin film of Matrigel (Fig. 2C). Results showed significant expression of constitutive endothelial proteins, such as CD31 (67.2%), VE-cadherin (58.8%), and VEGFR2 (37.8%), as well as a triple-positive population (16.4%), although did not show a complete reduction in the stem cell markers SSEA4, c-kit, and CD44 (19.2%, 28.5%, and 60.5%, respectively). In addition, the differentiated cells were negative for the immunological marker HLA-DR (0.493%) and positive for HLA-ABC (96.4%).

Characterization of fibrin/PEG hydrogels

Fibrin hydrogels became opaque upon gelation, while fibrin/PEG hydrogels remained translucent (Fig. 3A).

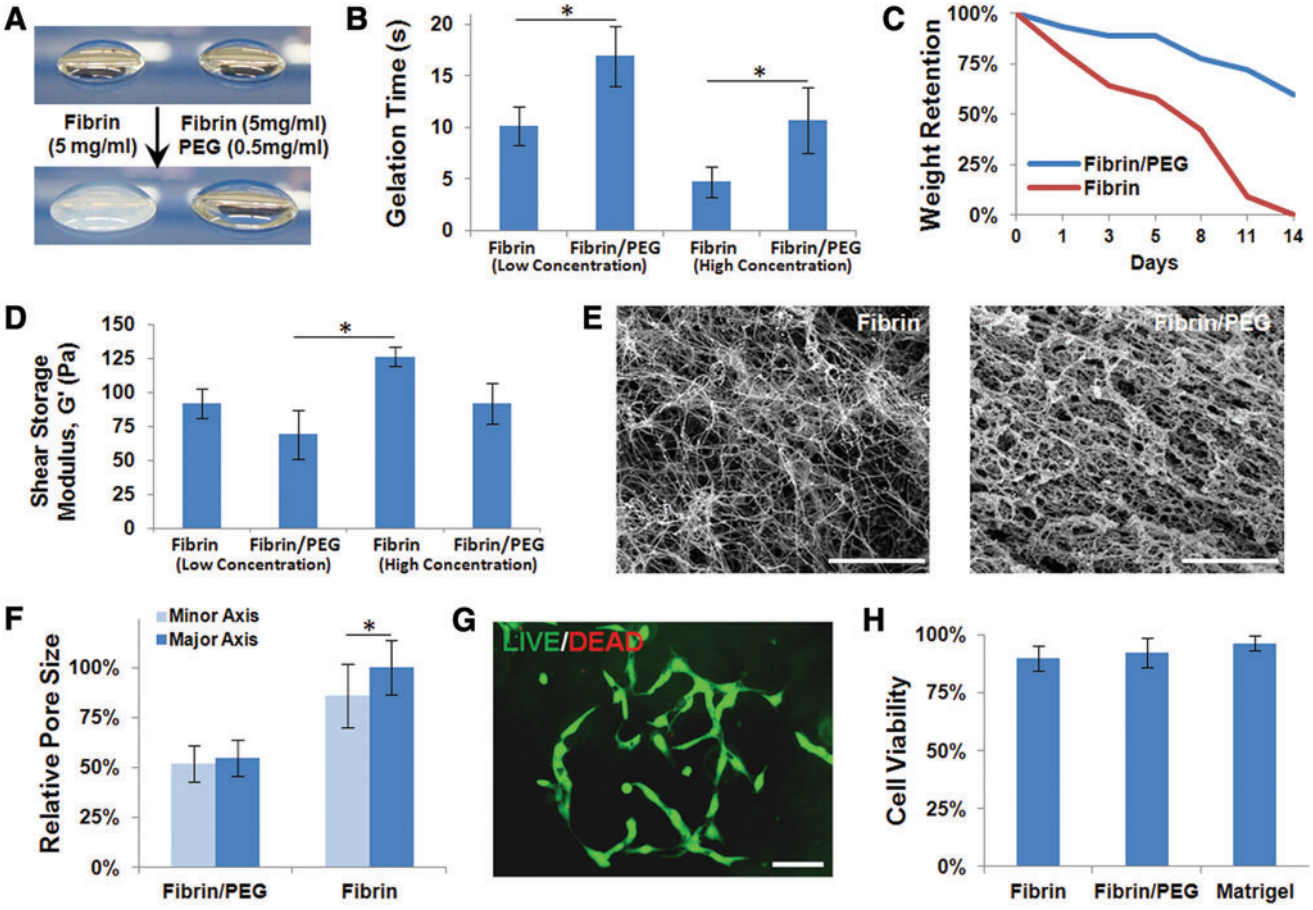

FIG. 3. Characterization of fibrin/PEG hydrogels. **(A)** Fibrin hydrogels became opaque upon gelation, while fibrin/PEG hydrogels remained translucent. **(B)** Gelation time of low-concentration fibrinogen (5 mg/mL) solutions at 37°C was on the order of seconds, while gelation of PEGylated fibrinogen (0.5 mg/mL PEG) was significantly slower. A similar effect was seen in higher concentration fibrinogen (10 mg/mL) and PEGylated fibrinogen gels (1.0 mg/mL PEG). **(C)** After 14 days *in vitro*, high-concentration fibrin-only scaffolds in media alone were completely degraded, while fibrin/PEG hydrogels remained intact. **(D)** The shear storage modulus (G′) of samples ranged from 50–150 Pa. Fibrin/PEG hydrogels were not significantly softer compared to fibrin-only hydrogels at either given concentration, although the higher concentration fibrin gels were significantly stiffer than the low-concentration fibrin/PEG gel. **(E)** Scanning electron microscope images revealed that fibrin-only hydrogels contained very thin fibrils, while fibrin/PEG hydrogels contained much larger bundled structures. Scale bars are 10 μm. **(F)** Pores throughout fibrin hydrogels were not uniform, as seen by significant differences in the major and minor pore axes. Overall pore sizes were significantly smaller in fibrin/PEG samples. **(G, H)** No significant difference was seen in AFSC attachment or viability after 7 days when comparing fibrin-only, fibrin/PEG, or Matrigel. A value of $p < 0.05$ (*) was considered significant in all tests. PEG, poly(ethylene glycol). Color images available online at www.liebertpub.com/tea

Gelation time of low-concentration fibrinogen solutions (5 mg/mL) at 37°C was on the order of seconds (10.1 ± 1.88 s), while gelation of PEGylated fibrinogen was significantly slower (16.9 ± 2.95 s, $p < 0.05$). A similar effect was seen in higher concentration fibrinogen (10 mg/mL) and PEGylated fibrinogen gels (4.71 ± 1.43 and 10.71 ± 3.17 s, respectively; $p < 0.05$) (Fig. 3B).

After 14 days *in vitro*, the weight retentions of high-concentration scaffolds in media alone were assessed. Fibrin-only hydrogels were completely degraded (0.4% ± 0.3% remaining), while fibrin/PEG hydrogels remained intact (65% ± 9%; $p < 0.05$) (Fig. 3C).

The shear storage modulus (G′) of samples ranged from 50–150 Pa. Fibrin/PEG hydrogels were not significantly softer compared to fibrin-only hydrogels at either given concentration (69.3 ± 18.1 vs. 91.9 ± 11.4 Pa at 5 mg/mL; 126.1 ± 7.5 vs. 91.8 ± 15.2 Pa at 10 mg/mL), although the higher concentration fibrin gels were significantly stiffer than the low-concentration fibrin/PEG gel (126.1 ± 7.5 vs. 69.3 ± 18.1 Pa; $p < 0.05$) (Fig. 3D).

SEM images revealed that fibrin-only hydrogels contained very thin fibrils (90 ± 3.9 nm thick), while fibrin/PEG hydrogels contained much thicker fibers (610 ± 33 μm thick) (Fig. 3E). Pores throughout fibrin hydrogels were not uniform, as seen by significant differences in the major and minor pore axes (1.64 ± 0.45 vs. 1.41 ± 0.52 μm for fibrin only, $p < 0.05$; 0.90 ± 0.30 vs. 0.85 ± 0.30 μm for fibrin/PEG). Overall pore sizes were significantly smaller in fibrin/PEG samples (0.88 ± 0.30 vs. 1.52 ± 0.48 μm, $p < 0.05$) (Fig. 3F). No significant difference was seen in AFSC attachment or viability after 7 days when comparing fibrin-only, fibrin/PEG, or Matrigel (89.9% ± 5.4%, 92.3% ± 6.5%, 96.4% ± 3.0%, respectively) (Fig. 3G, H).

Assessment of in vitro *network formation*

To determine the individual contribution of both AFSC-EC, our proposed vascular cell source, and AFSC, our proposed perivascular cell source, network formation by AFSC, AFSC-EC, MSC, HUVEC, and combinations thereof were analyzed when seeded in fibrin for 7 days (Fig. 4A), fibrin/PEG for 7 days (Fig. 4B), and fibrin/PEG for 14 days (Fig. 4C). All network parameters were normalized to HUVEC/MSC cocultures, which were considered the positive control for this study. Fluorescent staining of actin filaments was used to obtain a clear cellular outline and facilitate quantitative analysis (Fig. 5A). Data collected included assessment of average vessel length (Fig. 5E), thickness (Fig. 5F), and area (Fig. 5G), as well as the degree of branching (Fig. 5H).

When comparing the networks formed by AFSC-EC and HUVEC individually after 2 weeks in fibrin/PEG hydrogels, no statistically significant difference was seen (vessel length: 48.1% ± 10.5% vs. 46.0% ± 16.8%; vessel thickness 70.2% ± 21.3% vs. 74.8% ± 19.2%; vessel area: 55.3% ± 12.1% vs. 59.1% ± 15.2%; number of branch points: 47.0% ± 18.2% vs. 34.2% ± 9.34%; all normalized to HUVEC/MSC cocultures).

Coculturing AFSC-EC or HUVEC with either AFSC or MSC, while maintaining a constant seeding density, resulted in an increase in all measured network parameters. Compared to the previously listed values, the synergistic effects of AFSC and MSC on network formation by AFSC-EC

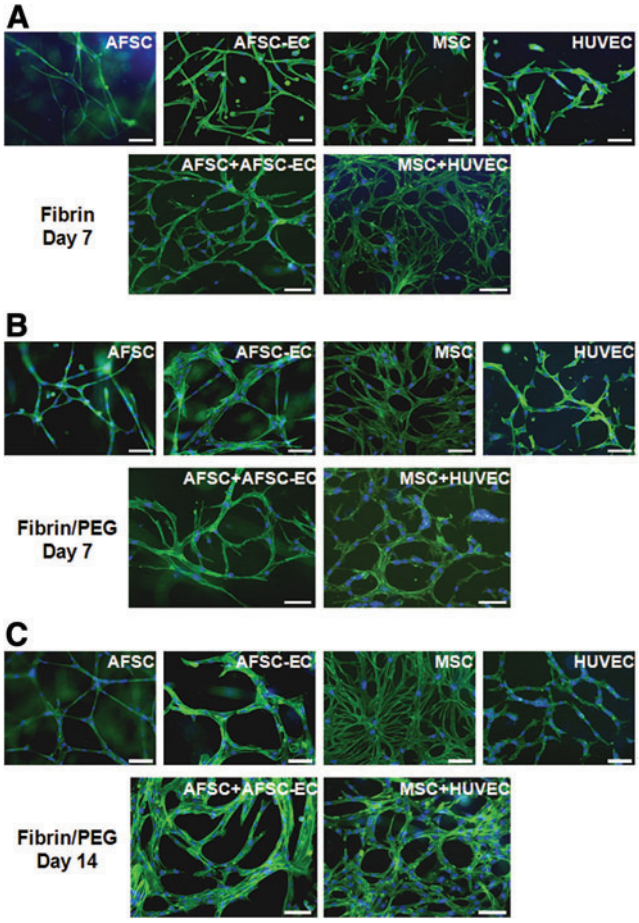

FIG. 4. Network formation within fibrin and fibrin/PEG hydrogels. AFSC, MSC, AFSC-EC, HUVEC, and cocultures were seeded and cultured *in vitro* within **(A)** fibrin for 7 days, **(B)** fibrin/PEG for 7 days, and **(C)** fibrin/PEG for 14 days. Actin filaments were labeled with phalloidin (*green*) and nuclei were counterstained with DAPI (*blue*). No fibrin-only day 14 samples were available due to degradation (see Fig. 3C). Scale bars are 100 μm. Color images available online at www.liebertpub.com/tea

(vessel length: 72.9% ± 26.7% and 59.1% ± 10.6%; vessel thickness: 109% ± 16.8% and 116% ± 38.0%; vessel area: 87.7% ± 12.4% and 82.5% ± 10.6%; number of branch points: 67.6% ± 17.0% and 57.9% ± 10.4%) and on network formation by HUVEC (vessel length: 105% ± 30.1% and 100% ± 19.7%, $p < 0.05$; vessel thickness: 111% ± 27.7% and 100% ± 15.4%; vessel area: 127% ± 23.8% and 100% ± 21.8%; number of branch points: 72.7% ± 23.8% and 100% ± 34.0%, $p < 0.05$) can clearly be seen; however, the effect of these potential perivascular cell sources was more pronounced on HUVEC than AFSC-EC in the cases of vessel length (102% ± 25% vs. 66.0% ± 18.7%, $p < 0.05$) and vessel area (114% ± 22.8% vs. 85.1% ± 11.5%, $p < 0.05$).

Fibrin/PEG hydrogels seeded with cocultures of either AFSC-EC/AFSC or HUVEC/MSC were sectioned and then stained with H&E, to assess the potential for lumen formation *in vitro* (Fig. 5B). H&E-stained slides showed fibrin scaffolds stained light pink and embedded cells stained dark pink/purple. The majority of AFSC-based slides (88%)

showed areas where branching cell networks were surrounding regions in which the fibrin/PEG scaffold was not present. The average diameter of the lumen-like regions in AFSC-derived networks was similar to that of HUVEC/MSC-derived networks (45.8 ± 6.3 vs. $54.2 \pm 9.7\,\mu m$, respectively). In select regions of the sectioned hydrogels, localization of aSMA and CD31 within embedded cells resembled that of immature capillary-like structures (Fig. 5C). Populations of AFSC and AFSC-EC were labeled with membrane-bound dyes pre-encapsulation and tracked as they proliferated and migrated through the fibrin/PEG hydrogels (Fig. 5D). Qualitatively, a clear interaction between AFSC and AFSC-EC was observed.

Discussion

The application of AFSC to the repair of congenital defects in neonates is especially promising because AF is routinely collected when a congenital defect is detected, with minimal risk,[23,24] and AFSC-derived cell constructs are genetically matched to the patient, significantly reducing the risk of immunorejection.[11,25] Surgical treatment of congenital abnormalities is often complicated by insufficient available tissue at the time of repair, resulting in the use of synthetic materials and a corresponding high morbidity rate.[26–30] Alternatively, broad potential for differentiation and high proliferation rates make AFSC well suited for use in regenerative medicine therapies such as engineered skeletal/cardiac muscles, tendons, heart valves, and blood vessels.[11,17,31–35]

This study confirms our previous work on the capacity for VEGF-mediated differentiation of c-kit$^+$ AFSC into endothelial-like cells,[14] as well as illustrates the vasculogenic and perivasculogenic potential of AFSC within a three-dimensional fibrin/PEG scaffold *in vitro*.

Several distinct subpopulations of AF-derived cells express multipotency markers, but c-kit$^+$ AFSC have been consistently shown to have the potential to differentiate into endothelial-like cells.[11,14,36] The subpopulation of CD31$^+$ cells within these c-kit-sorted AFSC is minor ($< 0.25\%$), but warrants further investigation to determine the degree of endothelial enrichment compared to endothelial differentiation. Recent studies suggest that 1 mL of human AF contains $\sim 10^4$ cells, 80% of which are viable, and 1% of which are c-kit$^+$.[27,37] Our laboratory has previously shown that c-kit$^+$ AFSC have a population doubling time of 36 h, which is supported in the literature.[26] In addition, routine second-trimester amniocentesis involves the removal of 12–15 mL of AF for analysis.[38] At this rate and starting volume, the generation of hundreds of millions of highly multipotent AFSC would be clinically feasible. As with all current stem cell therapies, patient variability is a critical hurdle. In an 86-patient trial, it was estimated that isolating c-kit$^+$ AFSC from second-trimester patients had a success rate of 71%.[39]

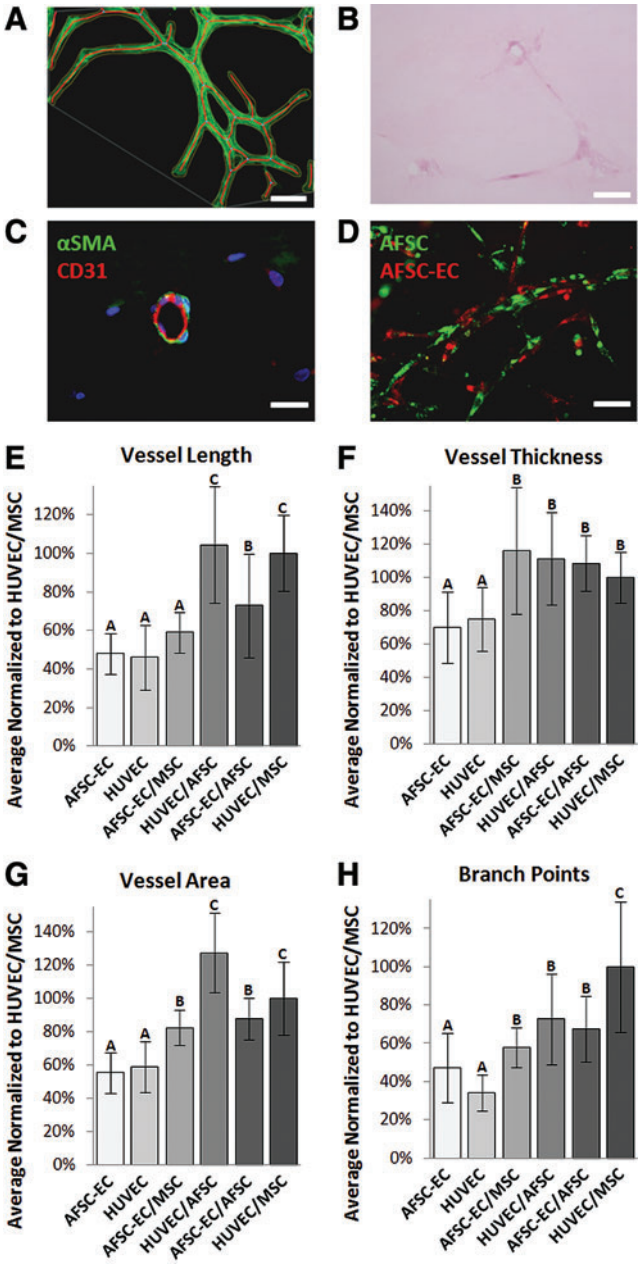

FIG. 5. Analysis of *in vitro* network formation within fibrin/PEG hydrogels. **(A)** Fluorescent staining of actin filaments was used to obtain a clear cellular outline and facilitate quantitative analysis. AFSC-derived network stained with phalloidin (*green*) and DAPI (*blue*) and then processed using AngioTool. Scale bar is 100 μm. Sections of paraffin-embedded AFSC coculture in fibrin/PEG hydrogel were stained with hematoxylin and eosin **(B**, scale bar is 150 μm) and αSMA/CD31 **(C**, scale bar is 50 μm) to assess the potential for lumen formation *in vitro*. Fibrin scaffolds stained *pink* and embedded cells stained *dark pink/purple*. In select regions, localization of αSMA and CD31 within embedded cells resembled that of immature capillary-like structures. **(D)** Populations of AFSC (*green*) and AFSC-EC (*red*) were labeled with membrane-bound dyes pre-encapsulation and tracked as they proliferated and migrated through the fibrin/PEG hydrogels. Scale bar is 100 μm. Data collected included assessment of **(E)** average vessel length, **(F)** thickness, and **(G)** area, as well as **(H)** the degree of branching. All network parameters were normalized to HUVEC/MSC cocultures. Bars that share a letter were not significantly different from each other. A value of $p < 0.05$ was considered significant in all tests. HUVEC, human umbilical vein endothelial cells. Color images available online at www.liebertpub.com/tea

As knowledge of the complex protein expression profile associated with these stem cells increases, more efficient sorting methods could provide a solution to this issue.

VEGF is often used as the primary stimulus for chemical-mediated endothelial differentiation of mesenchymal and embryonic stem cells,[40–42] and we have previously reported on the correlation between VEGF concentration and the development of endothelial-like phenotype by AFSC. Significant expression of constitutive endothelial proteins such as CD31, VE-cadherin, and VEGFR2 was seen in AFSC-EC, although it is again important to note batch-to-batch variability. AFSC-EC were HLA-DR negative and HLA-ABC positive, suggesting low immunogenicity. Additionally, a subpopulation of AFSC was unresponsive to the chemical stimulus in the endothelial media and did not show a complete reduction in the stem cell markers SSEA4, c-kit, and CD44. This can likely be attributed to the population of AFSC that do not express VEGFR2 and thus cannot respond to VEGF stimuli.

The fibrin/PEG scaffold provided a platform that was easily tunable and shown in the literature to be proangiogenic. The gelation rate could be modulated through calcium concentration, which affects the thrombin enzymatic activity. While this increases handleablity *in vitro*, it has significant implications for translation to injectable *in situ* technologies where stem cells have found utility. The solubilized hydrogel components are stable at 4°C for up to a week, further improving clinical viability.

PEG was utilized to decrease the degradation rate of fibrin-only scaffolds, which are not conducive to prevascularization strategies longer than a couple of weeks. We hypothesize that the reduction in degradation rate is driven by changes to the microscopic structure of the hydrogels. Specifically, the amorphous crosslinking of fibrin by the linear bi-functional PEG results in thicker fibers and smaller pores, which significantly reduce the surface area exposed to degradation. The differences in morphologies can be seen in SEM images, and the increased amorphous characteristic may be responsible for the translucent nature of the fibrin/PEG hydrogels. Throughout these changes, it was important to retain the bioactivity of the fibrin hydrogel component. Bulk stiffness, which is a critical cue for endothelial differentiation, and cell viability were both maintained throughout samples. Cell viability data are further supported by examples in the literature using this encapsulation method.[43–45] In addition, while the PEG variant used in these experiments is not biodegradable, the method of PEGylation used only allows for the covalent linking of PEG and fibrinogen, not multiple PEG chains. As the fibrin component of these scaffolds is hydrolyzed and enzymatically degraded, the attached PEG chains are expected to solubilize and clear as well. A 10:1 fibrinogen:PEG weight ratio and a uniform PEG distribution (as suggested by our SEM images) would indicate that PEG-rich areas, which have the potential to reduce cell attachment, were minimized.

The vasculogenic potential of cell-seeded scaffolds was assessed through the following network parameters: vessel length, area, and thickness and the number of branch points. Data for vessel length and area were captured for each image as a whole, then averaged, and are clear indicators of overall vascular robustness. Alternatively, thickness was analyzed on a per-vessel basis within each image and represents the average thickness of vessels between branches. By making this distinction, areas where two or more vessels temporarily merge are ignored to give a more accurate representation of individual vessel thickness. While the degree of branching is not necessarily an indicator of the quality of networks formed, it does provide information on network organization and allows for an additional level of comparison between cell types.

When comparing single cell type cultures within the fibrin/PEG hydrogels, no statistical difference in vessel formation was seen between AFSC-EC and HUVEC; however, both these groups displayed an increase in network parameters compared to AFSC or MSC cultures alone, suggesting AFSC-EC, like HUVEC, have significant vasculogenic potential. Cocultures containing either AFSC or MSC consistently displayed a more robust vessel formation compared to single cell types at a fixed seeding density, suggesting that AFSC, like MSC, play a synergistic role in network formation and have significant perivascular potential. Due to their similarities in morphology and gene expression, our hypothesis is that the secretome profile for AFSC is similar to what has been described in the literature for MSCs, which includes the potential release of VEGF, IL-6, IL-8, and MCP-1, all of which directly enhance endothelial cell survival and vascular formation.[46] A complete panel of cytokine expression will be critical for fully understanding the role of AFSC in vascularization.

Almost 90% of AFSC-EC/AFSC-sectioned slides captured branching cell networks with the lumen-like area present. The average diameter of these regions was similar to those of HUVEC/MSC cocultures and on the same scale as capillary networks. H&E sections were appropriate for determining the precise morphology and patency of these networks, while immunofluorescent staining for endothelial- and perivascular-specific markers was essential for understanding the cellular organization. Further analysis is necessary to quantify the concentration of functional lumen-forming vessels.

In this study, we demonstrated the following: fibrin/PEG hydrogels provide a platform for cell encapsulation that promotes biocompatibility, mechanical stability, and vasculogenesis; AFSC in cocultures act as a support cell source similar to MSC, promoting increased vessel length, area, and thickness; and AFSC-derived cell networks were clearly formed, with vessel thickness and coverage area similar to HUVEC/MSC-derived networks. Further analysis is needed to determine vessel maturity and the potential for *in vivo* viability.

Acknowledgments

The authors thank the Texas Children's Hospital's Maternal-Fetal Medicine Center for supplying the AF, Dr. Joel Moake for generously providing the HUVEC, the Baylor College of Medicine Breast Cancer Pathology Laboratory for their histology expertise, and Dr. Laura Suggs for guidance using the fibrin/PEG system. AngioTool is an open source software developed by the National Cancer Institute's Center for Cancer Research and made available by the National Institutes of Health.

Grants

This study was supported by the NIH (O.M.B.), NSFGRFP (J.P.C.), NSF CAREER (J.G.J), and the Virginia

and L.E. Simmons Family Foundation (J.G.J). This project was also supported by the Cytometry and Cell Sorting Core at Baylor College of Medicine with funding from the NIH (AI036211, CA125123, and RR024574) and the assistance of Joel M. Sederstrom, and the Pathology and Histology Core at Baylor College of Medicine with funding from the NIH (NCI P30-CA125123).

Disclosure Statement

There are no competing financial interests.

References

1. Novosel, E.C., Kleinhans, C., and Kluger, P.J. Vascularization is the key challenge in tissue engineering. Adv Drug Deliv Rev **63,** 300, 2011.
2. Carmeliet, P., and Jain, R.K. Angiogenesis in cancer and other diseases. Nature **407,** 249, 2000.
3. Jain, R.K., Au, P., Tam, J., Duda, D.G., and Fukumura, D. Engineering vascularized tissue. Nat Biotechnol **23,** 821, 2005.
4. Laschke, M.W., Harder, Y., Amon, M., Martin, I., Farhadi, J., Ring, A., Torio-Padron, N., Schramm, R., Rucker, M., Junker, D., Haufel, J.M., Carvalho, C., Heberer, M., Germann, G., Vollmar, B., and Menger, M.D. Angiogenesis in tissue engineering: breathing life into constructed tissue substitutes. Tissue Eng **12,** 2093, 2006.
5. Laschke, M.W., Vollmar, B., and Menger, M.D. Inosculation: connecting the life-sustaining pipelines. Tissue Eng Part B Rev **15,** 455, 2009.
6. Clark, E. Microscopic observations on the growth of blood capillaires in the living mammal. Am J Anat **64,** 251, 1939.
7. Zarem, H.A. The microcirculatory events within full-thickness skin allografts (homografts) in mice. Surgery **66,** 392, 1969.
8. Orr, A.W., Elzie, C.A., Kucik, D.F., and Murphy-Ullrich, J.E. Thrombospondin signaling through the calreticulin/LDL receptor-related protein co-complex stimulates random and directed cell migration. J Cell Sci **116,** 2917, 2003.
9. Malda, J., Rouwkema, J., Martens, D.E., Le Comte, E.P., Kooy, F.K., Tramper, J., van Blitterswijk, C.A., and Riesle, J. Oxygen gradients in tissue-engineered PEGT/PBT cartilaginous constructs: measurement and modeling. Biotechnol Bioeng **86,** 9, 2004.
10. Kreutziger, K.L., Muskheli, V., Johnson, P., Braun, K., Wight, T.N., and Murry, C.E. Developing vasculature and stroma in engineered human myocardium. Tissue Eng Part A **17,** 1219, 2011.
11. De Coppi, P., Bartsch, G., Jr., Siddiqui, M.M., Xu, T., Santos, C.C., Perin, L., Mostoslavsky, G., Serre, A.C., Snyder, E.Y., Yoo, J.J., Furth, M.E., Soker, S., and Atala, A. Isolation of amniotic stem cell lines with potential for therapy. Nat Biotechnol **25,** 100, 2007.
12. Pok, S., Benavides, O.M., Hallal, P., and Jacot, J.G. Use of myocardial matrix in a chitosan-based full-thickness heart patch. Tissue Eng Part A **20,** 1877, 2014.
13. Pok, S., and Jacot, J.G. Biomaterials advances in patches for congenital heart defect repair. J Cardiovasc Transl Res **4,** 646, 2011.
14. Benavides, O.M., Petsche, J.J., Moise, K.J., Jr., Johnson, A., and Jacot, J.G. Evaluation of endothelial cells differentiated from amniotic fluid-derived stem cells. Tissue Eng Part A **18,** 1123, 2012.
15. Lozito, T.P., Kuo, C.K., Taboas, J.M., and Tuan, R.S. Human mesenchymal stem cells express vascular cell phenotypes upon interaction with endothelial cell matrix. J Cell Biochem **107,** 714, 2009.
16. Tsai, M.S., Lee, J.L., Chang, Y.J., and Hwang, S.M. Isolation of human multipotent mesenchymal stem cells from second-trimester amniotic fluid using a novel two-stage culture protocol. Hum Reprod **19,** 1450, 2004.
17. In 't Anker, P.S., Scherjon, S.A., Kleijburg-van der Keur, C., Noort, W.A., Claas, F.H., Willemze, R., Fibbe, W.E., and Kanhai, H.H. Amniotic fluid as a novel source of mesenchymal stem cells for therapeutic transplantation. Blood **102,** 1548, 2003.
18. Zhang, G., and Suggs, L.J. Matrices and scaffolds for drug delivery in vascular tissue engineering. Adv Drug Deliv Rev **59,** 360, 2007.
19. Jiang, B., Waller, T.M., Larson, J.C., Appel, A.A., and Brey, E.M. Fibrin-loaded porous poly(ethylene glycol) hydrogels as scaffold materials for vascularized tissue formation. Tissue Eng Part A **19,** 224, 2013.
20. Zhang, G., Wang, X., Wang, Z., Zhang, J., and Suggs, L. A PEGylated fibrin patch for mesenchymal stem cell delivery. Tissue Eng **12,** 9, 2006.
21. Zhang, G., Hu, Q., Braunlin, E.A., Suggs, L.J., and Zhang, J. Enhancing efficacy of stem cell transplantation to the heart with a PEGylated fibrin biomatrix. Tissue Eng Part A **14,** 1025, 2008.
22. Seetharaman, S., Natesan, S., Stowers, R.S., Mullens, C., Baer, D.G., Suggs, L.J., and Christy, R.J. A PEGylated fibrin-based wound dressing with antimicrobial and angiogenic activity. Acta Biomater **7,** 2787, 2011.
23. Jauniaux, E., and Rodeck, C. Use, risks and complications of amniocentesis and chorionic villous sampling for prenatal diagnosis in early pregnancy. Early Pregnancy **1,** 245, 1995.
24. Johnson, J.M., Wilson, R.D., Singer, J., Winsor, E., Harman, C., Armson, B.A., Benzie, R., Dansereau, J., Ho, M.F., Mohide, P., Natale, R., and Okun, N. Technical factors in early amniocentesis predict adverse outcome. Results of the Canadian Early (EA) versus Mid-trimester (MA) Amniocentesis Trial. Prenat Diagn **19,** 732, 1999.
25. Bossolasco, P., Montemurro, T., Cova, L., Zangrossi, S., Calzarossa, C., Buiatiotis, S., Soligo, D., Bosari, S., Silani, V., Deliliers, G.L., Rebulla, P., and Lazzari, L. Molecular and phenotypic characterization of human amniotic fluid cells and their differentiation potential. Cell Res **16,** 329, 2006.
26. De Coppi, P. Regenerative medicine for congenital malformations. J Pediatr Surg **48,** 273, 2013.
27. Kaviani, A., Perry, T.E., Dzakovic, A., Jennings, R.W., Ziegler, M.M., and Fauza, D.O. The amniotic fluid as a source of cells for fetal tissue engineering. J Pediatr Surg **36,** 1662, 2001.
28. de Kort, L.M., and Bax, K.M. Prosthetic patches used to close congenital diaphragmatic defects behave well: a long-term follow-up study. Eur J Pediatr Surg **6,** 136, 1996.
29. Schnitzer, J.J., Kikiros, C.S., Short, B.L., O'Brien, A., Anderson, K.D., and Newman, K.D. Experience with abdominal wall closure for patients with congenital diaphragmatic hernia repaired on ECMO. J Pediatr Surg **30,** 19, 1995.
30. Disa, J.J., Klein, M.H., and Goldberg, N.H. Advantages of autologous fascia versus synthetic patch abdominal reconstruction in experimental animal defects. Plast Reconstr Surg **97,** 801, 1996.
31. Bollini, S., Pozzobon, M., Nobles, M., Riegler, J., Dong, X., Piccoli, M., Chiavegato, A., Price, A.N., Ghionzoli, M., Cheung, K.K., Cabrelle, A., O'Mahoney, P.R., Cozzi, E.,

Sartore, S., Tinker, A., Lythgoe, M.F., and De Coppi, P. *In vitro* and *in vivo* cardiomyogenic differentiation of amniotic fluid stem cells. Stem Cell Rev **7,** 364, 2011.
32. Decembrini, S., Cananzi, M., Gualdoni, S., Battersby, A., Allen, N., Pearson, R.A., Ali, R.R., De Coppi, P., and Sowden, J.C. Comparative analysis of the retinal potential of embryonic stem cells and amniotic fluid-derived stem cells. Stem Cells Dev **20,** 851, 2011.
33. De Coppi, P., Callegari, A., Chiavegato, A., Gasparotto, L., Piccoli, M., Taiani, J., Pozzobon, M., Boldrin, L., Okabe, M., Cozzi, E., Atala, A., Gamba, P., and Sartore, S. Amniotic fluid and bone marrow derived mesenchymal stem cells can be converted to smooth muscle cells in the cryo-injured rat bladder and prevent compensatory hypertrophy of surviving smooth muscle cells. J Urol **177,** 369, 2007.
34. Rota, C., Imberti, B., Pozzobon, M., Piccoli, M., De Coppi, P., Atala, A., Gagliardini, E., Xinaris, C., Benedetti, V., Fabricio, A.S., Squarcina, E., Abbate, M., Benigni, A., Remuzzi, G., and Morigi, M. Human amniotic fluid stem cell preconditioning improves their regenerative potential. Stem Cells Dev **21,** 1911, 2012.
35. Delo, D.M., De Coppi, P., Bartsch, G., Jr., and Atala, A. Amniotic fluid and placental stem cells. Methods Enzymol **419,** 426, 2006.
36. Cananzi, M., and De Coppi, P. CD117(+) amniotic fluid stem cells: state of the art and future perspectives. Organogenesis **8,** 77, 2012.
37. Murphy, S.V., and Atala, A. Amniotic fluid and placental membranes: unexpected sources of highly multipotent cells. Semin Reprod Med **31,** 62, 2013.
38. Tharmaratnam, S., Sadek, S., Steele, E.K., Harper, M.A., Stewart, F.J., Nevin, J., Nevin, N.C., and Dornan, J.C. Early amniocentesis: effect of removing a reduced volume of amniotic fluid on pregnancy outcome. Prenat Diagn **18,** 773, 1998.
39. Guan, T., Chen, X.L., Wei, Y.J., Lai, Y., Xie, L.Y., Liu, Z.Y., Zhang, X.M., Liu, H.Q., Zhang, J.J., Xie, X.Y., and Liu, S.L. [Isolation and biological characterization of human amniotic fluid-derived stem cells]. Sichuan Da Xue Xue Bao Yi Xue Ban (J Sichuan Univ Med Sci Ed) **43,** 15, 2012.
40. Nourse, M.B., Halpin, D.E., Scatena, M., Mortisen, D.J., Tulloch, N.L., Hauch, K.D., Torok-Storb, B., Ratner, B.D., Pabon, L., and Murry, C.E. VEGF induces differentiation of functional endothelium from human embryonic stem cells: implications for tissue engineering. Arterioscler Thromb Vasc Biol **30,** 80, 2010.
41. Oswald, J., Boxberger, S., Jorgensen, B., Feldmann, S., Ehninger, G., Bornhauser, M., and Werner, C. Mesenchymal stem cells can be differentiated into endothelial cells *in vitro*. Stem Cells **22,** 377, 2004.
42. Tokalov, S.V., Gruner, S., Schindler, S., Wolf, G., Baumann, M., and Abolmaali, N. Age-related changes in the frequency of mesenchymal stem cells in the bone marrow of rats. Stem Cells Dev **16,** 439, 2007.
43. Galler, K.M., Cavender, A.C., Koeklue, U., Suggs, L.J., Schmalz, G., and D'Souza, R.N. Bioengineering of dental stem cells in a PEGylated fibrin gel. Regen Med **6,** 191, 2011.
44. Zamora, D.O., Natesan, S., Becerra, S., Wrice, N., Chung, E., Suggs, L.J., and Christy, R.J. Enhanced wound vascularization using a dsASCs seeded FPEG scaffold. Angiogenesis **16,** 745, 2013.
45. Zhang, G., Drinnan, C.T., Geuss, L.R., and Suggs, L.J. Vascular differentiation of bone marrow stem cells is directed by a tunable three-dimensional matrix. Acta Biomater **6,** 3395, 2010.
46. Ranganath, S.H., Levy, O., Inamdar, M.S., and Karp, J.M. Harnessing the mesenchymal stem cell secretome for the treatment of cardiovascular disease. Cell Stem Cell **10,** 244, 2012.

Address correspondence to:
Jeffrey G. Jacot, PhD
Department of Bioengineering
Rice University
6500 Main St.–MS 142
Houston, TX 77005

E-mail: jeff.jacot@rice.edu

Received: May 26, 2014
Accepted: November 14, 2014
Online Publication Date: January 27, 2015